Molecular three-terminal devices: fabrication and measurements

Herre S. J. van der Zant,*[a] Yann-Vai Kervennic,[a] Menno Poot,[a] Kevin O'Neill,[a] Zeger de Groot,[a] Jos M. Thijssen,[a] Hubert B. Heersche,[a] Nicolai Stuhr-Hansen,[b] Thomas Bjørnholm,[b] Daniel Vanmaekelbergh,[c] Cornelis A. van Walree[d] and Leonardus W. Jenneskens[d]

Received 3rd May 2005, Accepted 30th June 2005
First published as an Advance Article on the web 30th September 2005
DOI: 10.1039/b506240n

Incorporation of a third, gate electrode in the device geometry of molecular junctions is necessary to identify the transport mechanism. At present, the most popular technique to fabricate three-terminal molecular devices makes use of electromigration. Although it is a statistical process, we show that control over the gap resistance can be obtained. A detailed analysis of the current–voltage characteristics of gaps without molecules, however, shows that they reveal features that can mistakenly be attributed to molecular transport. This observation raises questions about which gaps with molecules can be disregarded and which not. We show that electrical characteristics can be controlled by the rational design of the molecular bridge and that vibrational modes probed by electrical transport are of potential interest as molecular fingerprints.

Introduction

Control of the molecular conductance by a third electrode is not only a necessary requirement for integration of molecular devices[1] in circuits, but also essential for a thorough study of transmolecular conduction. To date, three-terminal molecular devices have been fabricated by several approaches mostly based on lithographic techniques. These include electromigration[2] in which a metal wire is broken with an electric field, shadow evaporation[3] and electrochemical techniques.[4–7] In all these cases, nanoscale gaps are produced in metallic wires that are bridged by molecules, sitting on top of a gate electrode separated by an oxide layer. The gate electrode electrostatically modifies the potential of the molecular orbitals independently from the bias voltage. With the gate, the molecule can be oxidized or reduced and tuned between nonconducting and conducting states.[8–12]

The extent to which the orbital levels can be shifted up and down is controlled by the gate coupling parameter. This parameter is related to the gain of the device and in Coulomb theory it equals the ratio of the gate capacitance to the total capacitance of the islands. In an experiment, it should be close to unity in order to access different charge states. The geometry plays an important role in the gate coupling and one should take care that the electrodes themselves do not screen the gate potential. For example, when using electro-deposition to create nanogaps, three-dimensional growth usually occurs and structures may be created that are effective screens (see Fig. 1a).

[a] *Kavli Institute of Nanoscience, Delft University of Technology, PO Box 5046, 2600 GA, The Netherlands. E-mail: herre@qt.tn.tudelft.nl*
[b] *Nano-Science Center & Department of Chemistry, University of Copenhagen, Universitetsparken 5, DK-2100 Ø, Denmark*
[c] *Condensed Matter and Interfaces, Debye Institute, Utrecht University, Princetonplein 1, 3584 CC Utrecht, The Netherlands*
[d] *Organic Chemistry and Catalysis, Debye Institute, Utrecht University, Padualaan 8, 3584 CH Utrecht, The Netherlands*

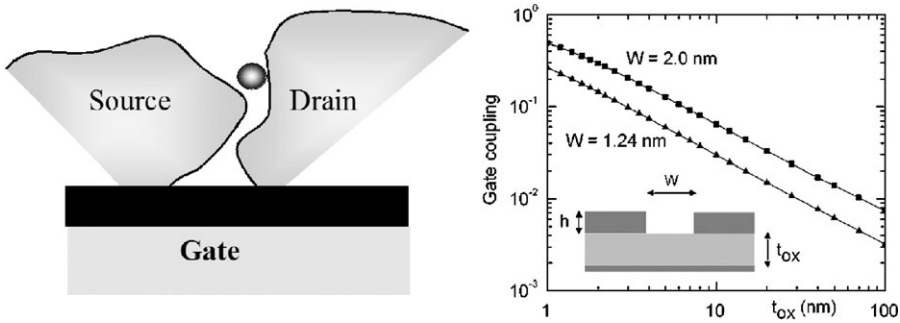

Fig. 1 Left: For the nano-object trapped in between two metallic electrodes fabricated for example by three-dimensional electro-deposition growth, the two leads can be effective screens against the gate. Right: gate coupling as a function of oxide thickness for two different gap sizes W. Calculation performed by solving Laplace's equation for the geometry shown in the inset with $\varepsilon_r = 9$ and $h = 0.6$ nm.

The molecule–electrode distance and the break-through voltage of the gate oxide are other important parameters. Currently, two gate materials are frequently used: heavily doped silicon substrates with thermally grown SiO_x on top and aluminium strips with a native oxide of only a few nanometers. In Fig. 1b, we plot the gate-coupling factor calculated from Laplace's equation for a 1.24 and 2 nm wide junction as a function of the gate oxide thickness. For large thicknesses the dependence is $\sim 1/t_{ox}$. For the aluminium gates with $\varepsilon_r = 9$, the gate coupling is about 0.1 so that with a typical break voltage of 4 V at low temperatures, the potential of the molecular levels can be shifted by ± 0.4 eV. For a silicon device ($\varepsilon_r \approx 3$) with an oxide thickness of 250 nm, extrapolation yields a gate coupling of about 10^{-3}. With a typical breakthrough voltage of 100 V, the range over which the potential on the molecule can be varied equals ± 0.1 eV. Here, we have not corrected for the different relative permeability of the two oxides. Calculations show that this is a small effect.

Wire fabrication

We have developed two techniques to create nanogaps on top of aluminium gates: electro-chemical etching and electromigration. The former method uses a combination of e-beam lithography and electrochemical etching. The approach allows the creation of gaps with subnanometer precision by *in situ* monitoring of the gap conductance during etching. Details of this technique are documented elsewhere.[7]

Electromigration is currently a widely adapted technique to fabricate molecular junctions and is reported to be a statistical method with poor control over the gap size.[2] We have extensively studied this electromigration method and found that some control can be obtained. We will now outline our method in more detail starting with device fabrication. In short, it consists of four lithographic steps. In the first step, contact pads and wide wires are defined by evaporation of 3 nm Ti, 35 nm Au and 15 nm AuPd. Secondly, the aluminium gate electrode is defined. The one-micron wide electrode is 50 nm thick with a sticking layer of 3 nm Ti. When taken out of the vacuum chamber of the evaporator, the aluminium oxidizes in air. The native oxide is typically 3 nm thick. The third step involves the definition of the thin and narrow gold wire that will be broken. A 10–12 nm thick and typically 100 nm wide gold wire without sticking layer is evaporated on top of the aluminium gate. In the last step, the thin wire is connected to the coarse pads by evaporation of 110 nm of AuPd.

Electromigration: Gap fabrication

The electrical circuit that is used to break the wire is shown in Fig. 2. It consists of a voltage source with a resistor in series, R_s. The current through the gold wire increases by ramping the voltage of the source; the current is determined by measuring the voltage across the series resistance. Electromigration-induced breaking[13] in gold is dominated by momentum transfer from charge carriers to the atoms, which is directed opposite to the electric field. The corresponding force is proportional to the current density and breaking occurs above a certain threshold value.

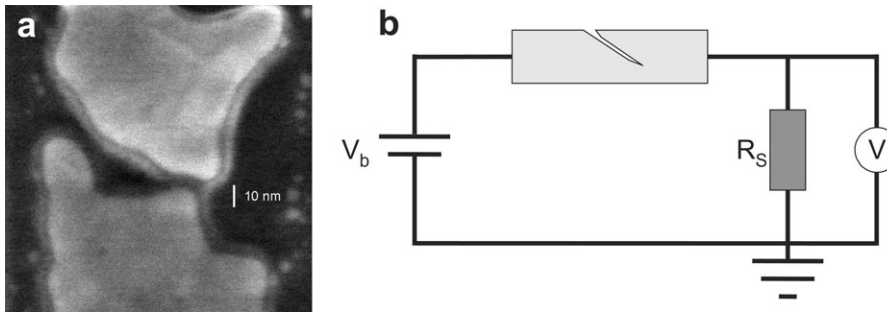

Fig. 2 Left: Scanning electron microscopy (SEM) picture of an electromigrated gold wire on top of an aluminium gate. The gap is smaller than a few nanometers. Right: Electrical circuit used to break the thin metallic wires.

Experiments performed at 4.2 K demonstrate that the ratio between the series resistance and the resistance of the gold wiring on the chip plays a crucial role (see Fig. 3). Wires with a resistance of 80 Ω break completely when using $R_s = 1$ kΩ. With $R_s = 10$ Ω, they break only partially as illustrated in the left hand side of Fig. 3. The wire first breaks to a plateau of 1 kΩ and only after increasing the voltage to 0.6 V, the wire breaks completely.

To investigate the dependence of the zero-bias gap resistance on R_s, 26 Au wires on the same chip have been broken with different R_s. The resistance of the gold wires before breaking was approximately 50 Ω. Six wires are broken with $R_s = 10$ Ω, six with $R_s = 50$ Ω, six with $R_s = 100$ Ω, four with $R_s = 300$ Ω and four with $R_s = 500$ Ω. Immediately after breaking the wire, the voltage has been swept to zero. Fig. 4 (left) shows the break curves for the five different values of R_s. Higher values of R_s yield higher break voltages, while the current at which breaking occurs remains approximately constant as expected for electromigration. The zero-bias resistance of each broken wire is plotted in the figure on the right hand side of Fig. 4. A clear dependence is observed: the higher the series resistance in the electrical circuit, the larger the gap resistance.

The difference in breaking can be understood as follows. The circuit with a high R_s compared to the bridge resistance is equivalent to that of a current source in which the current is kept constant. When increasing the bias voltage, the junction cross section decreases and the current density increases thereby accelerating the electromigration process. Before breaking most of the voltage is across R_s; during breaking this voltage is transferred to the junction. For low series resistances on the other hand, the voltage drop is mainly across the junction during the whole breaking process (connection to a voltage source)—this results in a less powerful breaking compared to the high-series-resistance case.

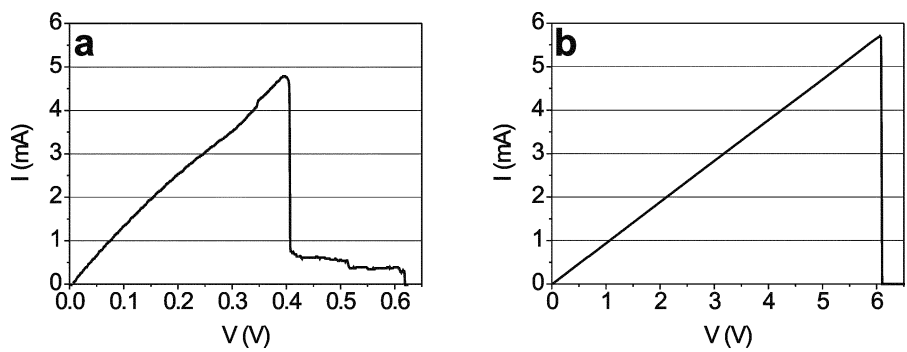

Fig. 3 Break curves for two different series resistances. The current, determined by measuring the voltage across R_s, as a function of the voltage that is ramped linearly in time. Left (a): Break curve for $R_s = 10$ Ω. The wire first breaks to a plateau of 1 kΩ before it breaks completely. Right (b): Break curve for $R_s = 1$ kΩ. The wire breaks completely.

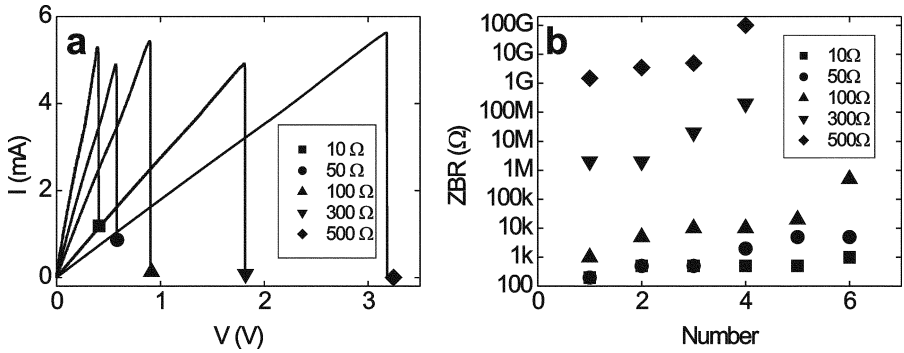

Fig. 4 Twenty six Au wires broken with five different R_s. The higher the series resistance, the higher the zero-bias resistance of the gap. Left (a): Representative break curves for different R_s, each represented with a different symbol. Right (b): Zero-bias resistance of each wire. Different symbols correspond to different R_s (see legend). The values within one set are ordered from left (low) to right (high).

A further improvement can be obtained by using an active feedback loop to monitor the resistance during breaking. While the electromigration process is inherently unpredictable, the catastrophic event that forms the void typically occurs in a timescale of ~ 100 μs—enough time to actively monitor the breaking process and adjust the voltage that is driving it. Different algorithms may be implemented to do this.[14,15] We ramp the voltage until a decrease in the absolute conductance is observed upon which the applied voltage is returned to zero and the loop is repeated until a desired resistance has been reached. Compared with simply ramping the voltage to a fixed limit, the yield of devices made with controlled electromigration is greatly increased from about 50% to more than 90%.

Current–voltage characteristics

To characterize the bare gold nanogaps, we have measured their current–voltage (*IV*) characteristics. A surprising result is that the *IV*'s curves generally do not follow the dependence expected from direct, through-space tunneling with its characteristic sinh(*V*) form.[18] We have collected the *IV*'s in seven different categories: (1) *IV*'s that do not show a current (<1 pA for $V = 100$ mV) indicating that the gap distance is a few nanometers or larger, (2) *IV*'s that are linear, (3) *IV*'s that show a suppression (ZBS) of the current at low bias[16] (see Fig. 5a), (4) smooth asymmetric *IV*'s (see Fig. 5b), (5) *IV*'s with steps (see Fig. 5c), (6) *IV*'s that are consistent with Coulomb blockade[17] (CB) (see Fig. 5d,e), and (7) *IV*'s with a zero-bias enhancement (ZBE) of the conductance around zero-bias. A gate effect is observed for the *IV*'s with steps, with a zero-bias anomaly and *IV*'s consistent with CB. An important consequence of the absence of direct tunneling behavior is that we cannot directly relate the gap resistance to a particular gap size.

The relative occurrence of the different *IV*-types is visualized in Fig. 6. A substantial number of *IV*'s shows Coulomb blockade features. These not only include the *IV*'s with Coulomb blockade and a gate effect (CB) but also the *IV*'s with a gate-dependent zero-bias enhancement (ZBE) of the conductance indicative of a Kondo effect in an island with an odd number of electrons,[9,10,12] and the *IV*'s with steps that are reminiscent of transport through an island with asymmetric barriers (Steps). From Fig. 6, one can conclude that in at least one third of the cases, Coulomb blockade features are observed. Most likely, small islands in the form of gold grains are present in the gap region. A similar conclusion has been drawn by Consalez *et al.*[19] who detect fluorescence from small grains produced by electromigration and by Houck *et al.*[15] who report on the Kondo effect in bare gold electro-migrated junctions. The appearance of nanometer-sized gold grains near the gap is a problem if one wants to distinguish transport through molecules from that through grains: the energies to add or withdraw an electron may be of the same order in both cases.

We have also investigated the breaking process with wires that contain a self-assembled layer of OPV-3 molecules ((*E*,*E*)-1,4-Bis[4-(acetylthio)styryl]benzene; see Fig. 6). Prior to breaking, the

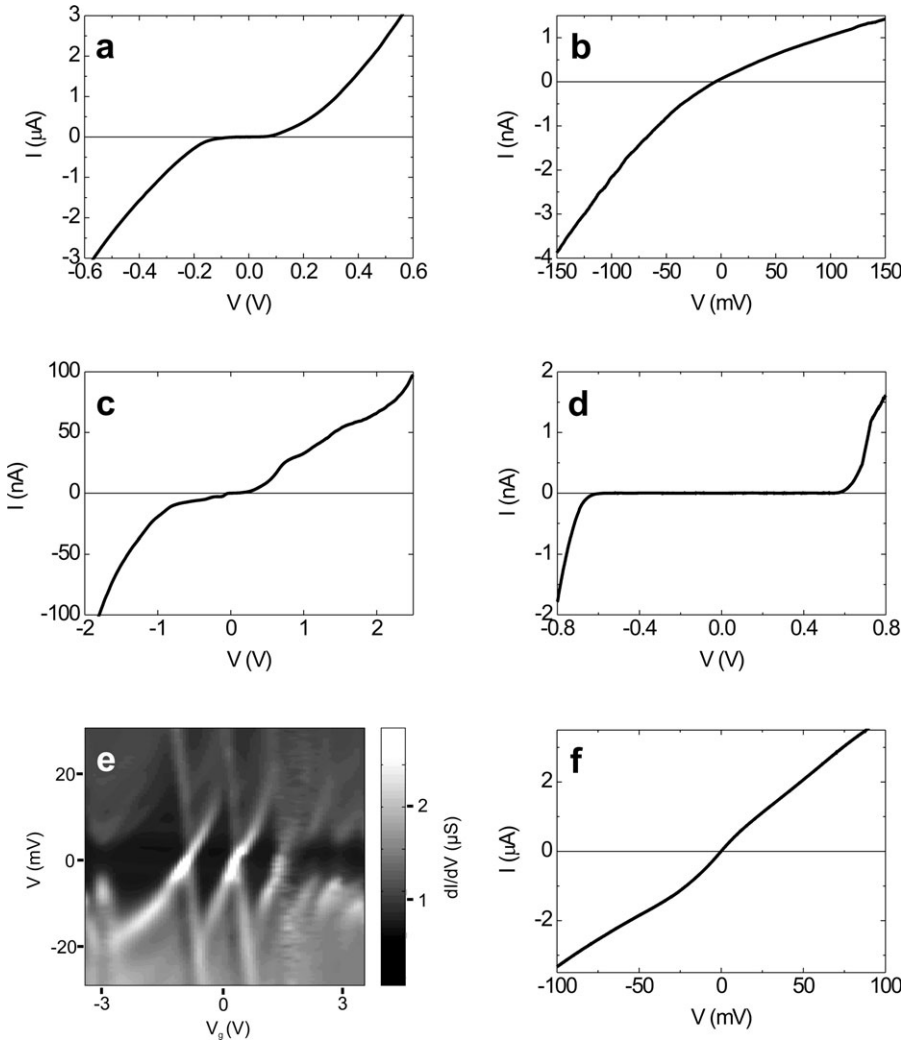

Fig. 5 Different types of current–voltage characteristics of bare gold nanogaps measured at 4.2 K: (a) *IV*'s with a zero-bias suppression (ZBS) of the current, (b) asymmetric, smooth *IV*'s, (c) *IV*'s with steps, (d) *IV*'s consistent with Coulomb blockade and (f) with a zero-bias enhancement of the conductance. In (e) a stability diagram of a sample with Coulomb blockade is shown. Plotted is dI/dV as a function of gate and bias voltage. In the black regions, the current is blocked (Coulomb diamond). Each black diamond-like structure corresponds to a different charge state.

wires are dipped in a 1 mM solution of OPV-3 in chloroform. Upon binding to gold, the acetate group falls off and the sulfur atom ensures a good bonding. After 12 h, the sample with typically 24 individual wires is rinsed with chloroform and blow-dried. Then it is transferred to the measuring set-up and cooled to 4.2 K, where the wires are broken. As a control measurement, we have measured nanogaps that were only dipped in the solvent for 12 h. Fig. 6 summarizes the result. Samples are all from the same fabrication run; measurements on other batches—not included—show similar behavior.

In all three types of junctions, in about one third of the cases no current is detected (<1 pA for $V = 100$ mV). In about one third of the cases, Coulomb blockade features (Steps, ZBE and CB) are seen. Surprisingly, samples that have been exposed to chloroform show more *IV*'s with a ZBE, but less *IV*'s with pure CB features. Another significant difference is that the samples with OPV-3 show

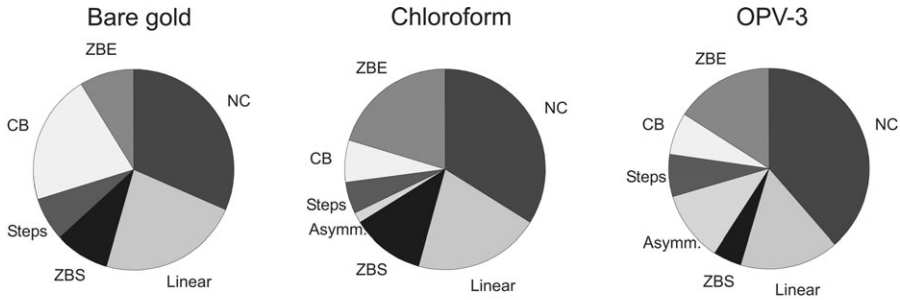

	Total	*NC*	*Linear*	*ZBS*	*Asymm.*	*Steps*	*CB*	*ZBE*
Bare gold	52	18	13	5	0	4	12	5
Chloroform	47	20	12	7	1	3	4	12
OPV-3	74	34	14	4	10	6	6	14

Fig. 6 Distribution of the different types of current–voltage characteristics measured on three different types of samples from the same fabrication run: bare gold wires, wires that have been exposed to the solvent for 12 h and wires that are exposed to the solvent with the OPV-3 molecules. NC stands for "no current", ZBS stands for "zero-bias suppression", Asymm. for "asymmetric *IV*", CB for "Coulomb blockade", and ZBE for "zero-bias enhancement". The table lists the number of junctions corresponding to each of the cases.

more asymmetric *IV*'s. These *IV*'s show no gate effect and their origin is unclear at the moment. From the comparison, we conclude that the breaking process itself and the measurement of current–voltage characteristics at low temperature do not provide statistical evidence for the presence of molecules in the gap.

Molecular junctions

As the current–voltage characteristics themselves do not provide clear signs for the presence of molecules inside the gap, the electromigration method raises questions about which samples can be disregarded and which not. Comparison of two batches, one with molecules and one without, may be inconclusive if the molecules influence the electro-migration process. Additional information is needed and in this respect a gate electrode is of crucial importance. The key question is what characteristic features can be used to distinguish molecular transport from transport through gold grains. It is important to note that at low temperatures up to now three-terminal measurements on molecular junctions have all shown Coulomb blockade features[8–12] including the Kondo effect.[9,10,12] Our measurements presented in the previous section, however, show that Coulomb blockade itself is not a distinctive feature. In the remainder of this paper, we present two measurements with different molecules that may provide information about the presence of molecules in the gap.

Molecular junctions with oligo(cyclohexylidene)

The sulfur end-functionalized oligo(cyclohexylidenes) molecules consist of cyclohexane rings[20] connected by double bonds. These are rigid molecules in which the sulfur-end atom in the cyclohexane rings binds strongly to gold atoms, leading to ordered self-assembled monolayers. Photo-induced charge transfer in Au/spacer/CdSe quantum dots assemblies[21] with the sulfur end-functionalized oligo(cyclohexylidenes) as molecular spacers has been measured at room temperature. Transport has been related to a favorable intramolecular interaction between the sulfur functionalities and the olefinic π orbitals, which are mediated by the σ C–C orbital system (through-bond interactions). Photo-electron spectroscopy[22] and photo-induced-electron transfer experiments[23,24] have confirmed the occurrence of transannular electronic interactions mediated *via* the σ–π–σ hydrocarbon skeleton.

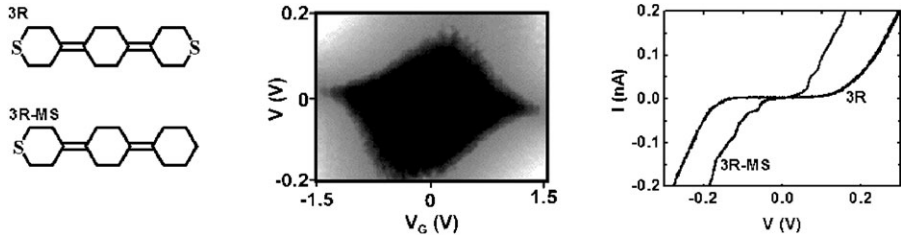

Fig. 7 Left: 3R molecules with two and one sulfur end groups. Middle: Stability diagram of a 3R sample measured at 8 K. Plotted is dI/dV as a function of bias and gate voltage. The conductance ranges from zero (dark) to 10 nS (light). Right: Two current–voltage characteristics measured at 10 K. The asymmetric junction with one sulfur end group (3R-MS) shows steps; the junction with the 3R molecule bonded to both electrodes by sulfur atoms exhibits a smooth curve.

Three-terminal devices were constructed with the technique that combines e-beam lithography and electrochemical etching.[7] Three different molecules were used: Molecules with two rings sulfur-functionalized at both ends, and three rings with either one sulfur or two sulfur termini. Here, we discuss results on junctions with the mono-sulfur three ring compound (3R-MS) and the three ring compound (3R) with two sulfur end atoms (see Fig. 7). It is important to note that junctions made with the same molecules share common features in their temperature dependence and gate effect.[25] No samples have been disregarded in contrast to the electromigration method. Furthermore, in the electrochemical method, the molecules are introduced after gap fabrication and the gap resistance before and after can be compared. In all cases a dramatic decrease of gap conductance has been observed. Control experiments show that the resistance decrease is due to the molecules.[7]

At room temperature, current–voltage (IV) characteristics of the molecular junctions are slightly nonlinear. The zero-bias room-temperature resistance varies from sample to sample between a few MΩ to 100 MΩ. One 3R-MS junction had a resistance of 500 MΩ. These differences may reflect variations in bonding strengths or in molecule–lead geometries, *i.e.*, in the exact chemisorption of the molecule on the gold. Another factor may be the number of molecules; we cannot be sure that only a single molecule is bound between the gold leads.

At low temperatures current–voltage characteristics are strongly nonlinear. Surprisingly, we consistently find that the IV's from the junctions with the asymmetric, 3R-MS molecules (3 studied) show steps whereas the junction with the symmetric 3R (5 studied of which 3 had the gate connected) do not. Fig. 7 shows an example. For the mono-sulfur three ring compound 3R-MS, the sulfur-functionalized site is well coupled to the gold electrode while the other side is—most likely—only weakly coupled through a van der Waals interaction. The set-up resembles the one of a scanning tunneling microscopy (STM) experiment in which the two barriers (tip–object and object–substrate) are very asymmetric. In STM experiments steps in the IV are generally observed and identified as Coulomb staircases.[26] In our case, steps may also be due to vibrational modes of the molecules (see also discussion next section).

When changing the voltage on the gate, a strong influence on the current is observed for both types of molecular junctions. For the asymmetric junction, we observe shifts in the step position but switches are often observed making a detailed analysis over the full gate range (± 2V) difficult. In contrast, gate dependent measurements on the symmetric junctions are stable. In Fig. 7 we plot the numerically obtained derivative dI/dV as a function of gate and bias voltage. The resulting stability diagram comprises more than one hundred curves. In the black region in the middle, current is below the measuring accuracy of one pA. From the diamond-like structure in Fig. 7 the value of the gate-coupling—estimated as half the diamond height divided by its width—equals about 0.1 in agreement with the calculated value of Fig. 1. Two other samples show similar stability diagrams as the one in Fig. 7 with similar gate coupling values.

The differential conductance plot does not show the features that are commonly observed in weakly coupled molecular junctions.[8–12] To be more specific, a surprising feature of the data in Fig. 7 is the absence of degeneracy points along the gate axis for low bias.[17] The crossing of a degeneracy point corresponds to the appearance of a new charge state. For sharp levels, this crossing is a well-

defined point in the stability diagram and when measuring for low bias the current as a function of gate, sharp current peaks occur. In our experiment on the other hand, we observe a steady increase of the current as the gate voltage is increased. Our data are therefore incompatible with the usual Coulomb blockade theory for weakly coupled systems.

The absence of degeneracy points in our junctions may be explained by the presence of substantially broadened HOMO and LUMO levels[27] due to a molecule–gold hybridization. In this respect, it is important to realize that the sulfur end-functionalities in the oligocyclohexylidenes interact effectively through the σ–π–σ framework. A favorable interaction between the sulfur lone pairs and the olefinic double bond exists.[22] The situation is different from that in aromatic thiols or sulfides, in which the sulfur lone pairs are more distant from the aromatic levels. The sulfur and aromatic moieties may therefore be effectively more decoupled leading to the formation of higher barriers at the molecule–lead contact and hence a weaker coupling.

Molecular junctions with OPV-3

With electromigration, junctions with the π-conjugated OPV-3 molecule are fabricated as outlined in the section on current–voltage characteristics. Thiol groups at both ends of this molecule (see Fig. 6) ensure a good bonding to the gold electrodes. In Fig. 8a, the differential conductance as a function of gate and bias voltage is shown (stability diagram). The plot shows one crossing point at a gate voltage of approximately −0.5 V associated with the separation of two charge states that differ by one electron. As the plot shows no indications of diamond edges that close again, the energy to add an additional electron (for both charge states) is well above 200 meV, the maximum bias applied in Fig. 8a.

The stability diagram shows a bright excitation running parallel to the diamond edges. It does not extend all the way to the diamond edge. Extrapolation to the diamond edge gives an energy of 50 meV for this excitation; its origin, however is unclear. The stability diagram also shows two black lines, symmetrically located around the $V = 0$ axis. Their color is black as they exhibit negative differential conductance as illustrated in Fig. 8b, in which a dI/dV curve taken at a gate voltage of −2 V is shown. On the left hand side of the plot the black lines appear at ±150 mV in the region where current is blocked and they are therefore due to an inelastic co-tunnel process.[28] In the case of an electronic excitation, cotunnel lines are expected to transfer into lines that run parallel to the diamond edges as they enter the region where current flows. In Fig. 8a this expected behavior is indicated by the dashed lines. Clearly, the data in Fig. 8 show a completely different pattern that does not follow straightforwardly from the usual Coulomb blockade theory.

Recently, Kushmerick *et al.*[29] have measured current–voltage characteristics of OPV-3 molecules in parallel in a crossed wire geometry. With inelastic tunneling spectroscopy (IETS), they have

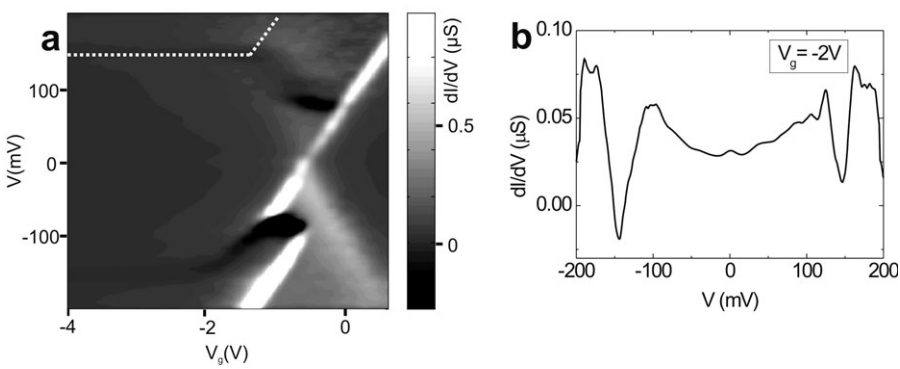

Fig. 8 (a) Large-bias stability diagram of a molecular junction with OPV-3 measured at 2 K. The plot shows one diamond crossing at a gate voltage of −0.5 V and at the left hand side two black horizontal lines whose position changes when reaching the Coulomb diamond edge. The dashed line indicates the expected behavior for an electronic excitation. (b) Differential conductance *vs.* bias voltage measured at a gate voltage of −2 V showing dips at approximately ±150 meV.

studied vibrational modes of OPV-3 molecules. Features in the second derivative are observed at 96, 134, 144, 174 and 195 mV. The mode at 144 mV is ascribed to a vibration of the benzene ring.

The question now arises: Can we assign the 150 meV feature we observe in the stability diagram to the same vibrational mode? This cannot easily be answered. Firstly, it should be emphasized that only one out of the 75 junctions with OPV-3 studied showed a stability diagram with the large addition energies and the 150 meV feature that are present in Fig. 8b. A second issue concerns the vibrational induced line shapes. In inelastic tunneling spectroscopy (IETS) one usually plots[29–32] the second derivative of the IV curves. Peaks then correspond to the location of the vibrational modes. It has theoretically been shown that also dips in the second derivative of the current–voltage characteristic may appear.[33] In Coulomb physics one expects a peak in the dI/dV as soon as a new electronic level enters the bias window. In the cotunnel regime, a step instead of a peak appears. For vibrational modes, the same general features are expected but electron–phonon coupling in movable dots is presently a field of intense study. For example, recent theoretical studies have shown that vibrational excitations may exhibit negative differential resistance when nonequilibrium processes associated with a strong electron–phonon coupling are present.[34] A more detailed understanding of the line shape is needed to be able to assign features in the current–voltage characteristics to vibrational modes of the molecule. Such studies should include the dependence of the vibrational energy on the gate voltage[32] and possibly on the charge state and the environment.

Conclusions

There are several approaches to contact single molecules. Each of them has its advantages and disadvantages. To determine the transport mechanism of molecular junctions, measurements with a gate provide crucial information. Planar technologies such as electromigration and electrochemical methods are usually adopted, but recently gates have also been incorporated in mechanical break junctions[35] and electrochemical gates have been used for single molecule transport at room temperature.[36]

With the planar techniques, it is very difficult to distinguish molecular transport from transport through small gold grains or other imperfections near the gap region. Although impressive improvement has been made in recent years, it is still not clear what the criteria are to determine molecular transport with a high degree of certainty. Inelastic-tunneling spectroscopy is an important tool that may be used as a molecular fingerprint, but a better understanding is necessary. A second strategy is to use molecule functionality. We have shown that the lead–molecule coupling can be used to make this distinction. Other routes include molecules with magnetic properties different from those expected for gold grains and light-sensitive molecules that switch conformation back and forth upon radiation with different wavelengths.

It is important to agree on which "molecular" fingerprints in the (I, V, V_G) characteristics must be observed before any conclusion can be made on the nature of the junction. Lastly, it would also be very helpful if measurements on molecular junctions fabricated with different techniques are compared with each other as well as with theoretical calculations.

Acknowledgements

We thank Edgar Osorio for discussions. Financial support is obtained from the Dutch Organization for Fundamental Research on Matter (FOM), the Danish Nanotechnology Program and by the EC through the FP6 program (contract no. FP6-2004-IST-003673). This publication reflects the views of the authors and not necessarily those of the EC. The Community is not liable for any use that may be made of the information contained herein. K. O'Neill acknowledges support of the EC under a Marie Curie Host for incoming International Fellowships.

References

1 C. Joachim, J. K. Gimzewski and A. Aviram, *Nature*, 2000, **408**, 541.
2 H. Park, A. K. L. Lim, A. P. Alivisatos, J. Park and P. L. McEuen, *Appl. Phys. Lett*., 1999, **75**, 301.
3 (*a*) K. Liu, Ph. Avouris, J. Bucchignano, R. Martel and S. Sun, *Appl. Phys. Lett*., 2002, **80**, 865; (*b*) M. S. M. Saifullah, T. Ondarçuhu, D. K. Koltsov, C. Joachim and M. E. Welland, *Nanotechnology*, 2002, **13**, 659.
4 C. Z. Li and N. J. Tao, *Appl. Phys. Lett*., 1998, **72**, 894.

5 A. F. Morpurgo, C. M. Marcus and D. B. Robinson, *Appl. Phys. Lett*., 1999, **74**, 2084.
6 Y. V. Kervennic, H. S. J. van der Zant, A. F. Morpurgo, L. Gurevich and L. P. Kouwenhoven, *Appl. Phys. Lett*., 2002, **80**, 321.
7 Y. V. Kervennic, D. Vanmakelbergh, L. P. Kouwenhoven and H. S. J. van der Zant, *Appl. Phys. Lett*., 2003, **83**, 3782.
8 H. Park, J. Park, A. K. L. Lim, E. H. Anderson, A. P. Allivisatos and P. L. McEuen, *Nature*, 2000, **407**, 57.
9 J. Park, A. N. Pasupathy, J. I. Goldsmith, C. Chang, Y. Yaish, J. R. Petta, M. Rinkoski, J. P. Sethna, H. D. Abruña, P. L. McEuen and D. C. Ralph, *Nature*, 2002, **417**, 722.
10 W. Liang, M. P. Shores, M. Bockrath, J. R. Long and H. Park, *Nature*, 2002, **417**, 725.
11 S. Kubatkin, A. Danilov, M. Hjort, J. Cornil, J.-L. A. L. Bredas, N. Stuhr-Hansen, P. Hedegård and T. Bjørnholm, *Nature*, 2003, **425**, 698.
12 L. H. Yu and D. Natelson, *Nano Lett*., 2004, **4**, 79.
13 (*a*) P. S. Ho and T. Kwok, *Rep. Prog. Phys*., 1989, **52**, 301; (*b*) M. Mahadevan and R. M. Bradley, *Phys. Rev. B*, 1999, **59**, 11037.
14 D. R. Strachan, D. E. Smith, D. E. Johnston, T.-H. Park, M. J. Therien, D. A. Bonneel and A. T. Johnson, *Appl. Phys. Lett*., 2005, **86**, 43109.
15 A. A. Houck, J. Labaziewicz, E. K. Chan, J. A. Folk and I. L. Chang, *Kondo effect in electromigrated break junctions, Cond-mat*, 2004, 410752.
16 The *IV*'s with a linear behavior at high current/voltage are consistent with Environmental Coulomb Blockade (see *e.g*. K. Flensberg., S. M. Girvin, M. Jonson, D. R. Penn and M. D. Stiles, *Phys. Scr., T*, 1992, **42**, 189) but more measurements (temperature dependence) are needed to draw definite conclusions.
17 See *e.g*., L. P. Kouwenhoven, D. G. Austing and S. Tarucha, *Rep. Prog. Phys*., 2001, **64**, 701.
18 J. G. Simmons, *J. Appl. Phys*., 1963, **34**, 1793.
19 J. Gonzales, T.-H. Lee, M. D. Barnes, Y. Antoku and R. M. Dickson, *Phys. Rev. Lett*., 2004, **93**, 147402.
20 F. J. Hoogesteger, R. W. A. Havenith, J. W. Zwikker, L. W. Jenneskens, H. Kooijman, N. Veldman and A. L. Spek, *J. Org. Chem*., 1995, **60**, 4375.
21 E. P. A. M. Bakkers, A. W. Marsman, L. W. Jenneskens and D. Vanmaekelbergh, *Angew. Chem., Int. Ed*., 2000, **39**, 2297.
22 A. W. Marsman, R. W. A. Havenith, S. Bethke, L. W. Jenneskens, R. Gleiter, J. H. van Lenthe, M. Lutz and A. L. Spek, *J. Org. Chem*., 2000, **65**, 4584.
23 F. J. Hoogesteger, C. A. van Walree, L. W. Jenneskens, M. R. Roest, J. W. Verhoeven, W. Schuddeboom, J. J. Piet and J. M. Warman, *Chem. – Eur. J*., 2000, **6**, 2948.
24 W. D. Oosterbaan, C. Koper, T. W. Braam, F. J. Hoogesteger, J. J. Piet, B. A. J. Jansen, C. A. van Walree, H. J. van Ramesdonk, M. Goes, J. W. Verhoeven, W. Schuddeboom, J. M. Warman and L. W. Jenneskens, *J. Phys. Chem. A*, 2003, **107**, 3612.
25 A comparison between the two and three ring molecular junctions can be found in: Y.-V. Kervennic, J. M. Thijssen, D. Vanmaekelbergh, R. Dabirian, C. A. van Walree, L. W. Jenneskens and H. S. J. van der Zant, *J. Am. Chem. Soc*., submitted.
26 See *e.g*., E. S. Soldatov, V. V. Khanin, A. S. Trifonov, D. E. Presnov, S. A. Yakovenko, G. B. Khomutov, C. P. Gubin and V. V. Kolesov, *JETP Lett*., 1996, **64**, 556.
27 The gate measurements suggest that the gold Fermi energy is approximately in the middle of the HOMO–LUMO gap. It is emphasized that in both cases only the tails of the levels are probed. The *IV* curves presented in this paper do not show this step, indicating that we only probe the rise of the current.
28 See *e.g*., S. De Franceschi, S. Sasaki, J. M. Elzerman, W. G. van der Wiel, S. Taracha and L. P. Kouwenhoven, *Phys. Rev. Lett*., 2001, **86**, 878.
29 J. G. Kusmerick, J. Lazorcik, C. H. Patterson, R. Shashidhar, D. S. Seferos and C. G. Bazan, *Nano Lett*., 2004, **4**, 639.
30 W. Wang, T. Lee, I. Kretzschmar and M. A. Reed, *Nano Lett*., 2004, **4**, 643.
31 R. H. M. Smit, Y. Noat, C. Untiedt, N. D. Lang, M. C. van Hemert and J. M. van Ruitenbeek, *Nature*, 2002, **419**, 906.
32 L. H. Yu, Z. K. Keane, J. W. Ciszek, L. Cheng, M. P. Stewart, J. M. Tour and D. Natelson, *Phys. Rev. Lett*., 2004, **93**, 266802.
33 M. Galperin, M. A. Ratner and A. Nitzan, *J. Chem. Phys*., 2004, **121**, 11965.
34 J. Koch and F. van Oppen, *Phys. Rev. Lett*., 2005, **94**, 206804.
35 A. R. Champagne, A. N. Pasupathy and D. C. Ralph, *Nano Lett*., 2005, **5**, 305.
36 B. Xu, X. Xia, X. Yang, L. Zang and N. Tao, *J. Am. Chem. Soc*., 2005, **127**, 2386.